

Structural insights into the effect of active-site mutation on the catalytic mechanism of carbonic anhydrase

Jin Kyun Kim,^a Cheol Lee,^a Seon Woo Lim,^a Jacob T. Andring,^b Aniruddha Adhikari,^a Robert McKenna^b and Chae Un Kim^{a*}

Received 22 March 2020
Accepted 11 August 2020

^aDepartment of Physics, Ulsan National Institute of Science and Technology (UNIST), Ulsan 44919, Republic of Korea, and ^bDepartment of Biochemistry and Molecular Biology, University of Florida, Gainesville, FL 32610, USA.
*Correspondence e-mail: cukim@unist.ac.kr

Edited by J. L. Smith, University of Michigan, USA

Keywords: carbonic anhydrase II; metalloenzymes; active-site mutation; active-site water dynamics; zinc ion; X-ray crystallography; enzyme mechanism; structural biology.

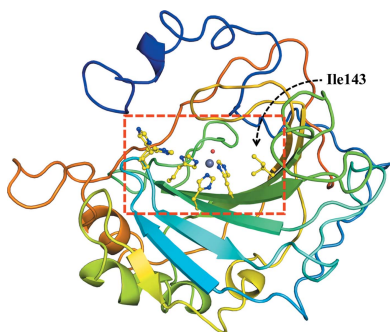
PDB references: human carbonic anhydrase II, native, 0 atm CO₂, 6km3; 7 atm CO₂, 6km4; 13 atm CO₂, 6km5; 15 atm CO₂, 6km6; V143I variant, 0 atm CO₂, 6klz; 7 atm CO₂, 6km0; 13 atm CO₂, 6km1; 15 atm CO₂, 6km2

Supporting information: this article has supporting information at www.iucrj.org

Enzymes are catalysts of biological processes. Significant insight into their catalytic mechanisms has been obtained by relating site-directed mutagenesis studies to kinetic activity assays. However, revealing the detailed relationship between structural modifications and functional changes remains challenging owing to the lack of information on reaction intermediates and of a systematic way of connecting them to the measured kinetic parameters. Here, a systematic approach to investigate the effect of an active-site-residue mutation on a model enzyme, human carbonic anhydrase II (CA II), is described. Firstly, structural analysis is performed on the crystallographic intermediate states of native CA II and its V143I variant. The structural comparison shows that the binding affinities and configurations of the substrate (CO₂) and product (HCO₃⁻) are altered in the V143I variant and the water network in the water-replenishment pathway is restructured, while the proton-transfer pathway remains mostly unaffected. This structural information is then used to estimate the modifications of the reaction rate constants and the corresponding free-energy profiles of CA II catalysis. Finally, the obtained results are used to reveal the effect of the V143I mutation on the measured kinetic parameters (k_{cat} and $k_{\text{cat}}/K_{\text{m}}$) at the atomic level. It is believed that the systematic approach outlined in this study may be used as a template to unravel the structure–function relationships of many other biologically important enzymes.

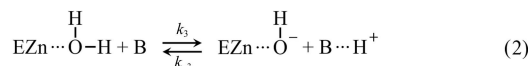
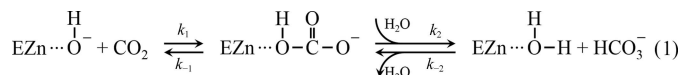
1. Introduction

Enzymes greatly enhance the catalytic rates of biochemical reactions compared with their uncatalyzed counterparts and are therefore essential to speed up biochemical processes (Jencks, 1987; Fersht, 1999; Frey & Hegeman, 2007). Enzyme active sites provide highly optimized microenvironments for their specific substrates by providing reactive groups such as nucleophiles or acids/bases that stabilize the transition state. Consequently, changes in the active-site residues can have large effects on enzyme activity. However, direct prediction of the impact of a single mutation on the activity of an enzyme remains challenging owing to the lack of precise correlations between the structure of the protein and its function at atomic resolution (Ishida, 2010). In this study, we describe the effect of a single amino-acid variation on a prototypical enzyme, human carbonic anhydrase II (CA II), by correlating its high-resolution reaction-intermediate structures with the measured kinetic parameters. Human carbonic anhydrases are well suited to serve as a model system for our study because their structures and active sites are well defined, and their overall



enzymatic mechanism is fairly straightforward and has been studied extensively (Krishnamurthy *et al.*, 2008).

Human carbonic anhydrases catalyze the reversible hydration/dehydration of $\text{CO}_2/\text{HCO}_3^-$ (Davenport, 1984; Christianson & Fierke, 1996; Chegwidan *et al.*, 2013; Frost & McKenna, 2013; Supuran & De Simone, 2015). In the CO_2 -hydration direction, the first step of catalysis is the conversion of CO_2 into HCO_3^- via the nucleophilic attack of a zinc-bound hydroxide. This reaction is followed by the displacement of the zinc-bound HCO_3^- by a water molecule (equation 1, where E stands for the enzyme; Silverman & Lindskog, 1988). The second step involves the transfer of a proton from the zinc-bound water to bulk solvent, regenerating the zinc-bound hydroxide (equation 2, where B stands for a general base: either a water or a proton-shuttling residue).



In CA II, the active-site zinc is located at the base of a 15 Å deep cleft and is tetrahedrally coordinated by three histidines (His94, His96 and His119) and a zinc-bound water (W_{Zn}) [Fig. 1(a)] (Christianson & Fierke, 1996). The active-site cavity is further subdivided into two distinct faces consisting of hydrophilic and hydrophobic residues. The hydrophilic face (Tyr7, Asn62, His64, Asn67, Thr199 and Thr200) of the active site coordinates the hydrogen-bonded water network (W1, W2, W3a and W3b) that connects the zinc-bound water to His64, the proton-shuttling residue [Fig. 1(b)] (Steiner *et al.*, 1975; Tu *et al.*, 1989; Nair & Christianson, 1991; Fisher *et al.*, 2005, 2010; Fisher, Maupin *et al.*, 2007; Fisher, Tu *et al.*, 2007; Maupin & Voth, 2007; Silverman & McKenna, 2007; Zheng *et al.*, 2008). It is known that the proton-transfer process is the rate-limiting step in CA II catalysis (Silverman & McKenna, 2007).

The hydrophobic face (Val121, Val143, Leu198, Val207 and Trp209) is located adjacent to the zinc-bound hydroxide and is responsible for substrate binding (Liang & Lipscomb, 1990; Domsic & McKenna, 2010). Leu198, Trp209 and Val121 constitute the mouth and sides of the hydrophobic pocket, while Val143 comprises the base of the hydrophobic pocket. A water molecule termed the ‘deep water’ (W_{DW}) is located at

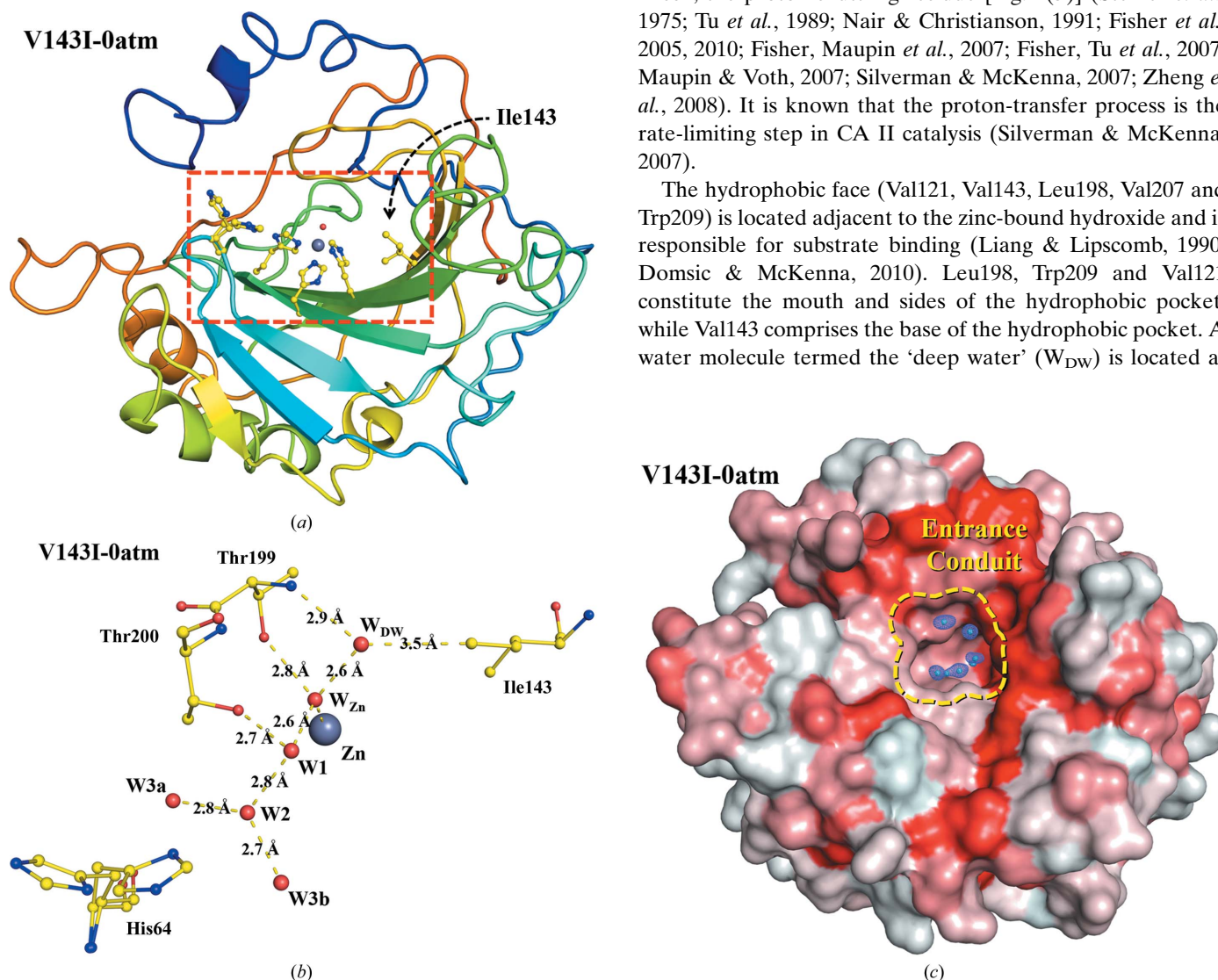


Figure 1 Structure of V143I CA II. (a) Overall structure of V143I CA II: V143I CA II with no CO_2 pressurization. The active site (red box) is located at a depth of 15 Å from the surface. Note that Ile143 is located at the hydrophobic pocket in the active site. (b) Ordered water network in the hydrophilic region serving as a proton-transfer pathway. (c) Surface rendition of V143I CA II. The entrance conduit (diameter of 7–10 Å, guided with a yellow dotted line) connects the active site to the bulk solvent outside, forming the replenishment pathway. The electron density of the entrance-conduit waters is contoured at 1.5σ . Hydrophobic amino acids are shaded in red, while hydrophilic amino acids are coloured white.

Table 1
Steady-state kinetic parameters for CO₂ hydration by native and V143I CA II.

	k_{cat}/K_m ($\mu\text{M}^{-1} \text{s}^{-1}$)	k_{cat} (μs^{-1})	K_m (mM)	k_1^\dagger ($\text{M}^{-1} \text{s}^{-1}$)	k_{-1}^\dagger (s^{-1})	k_2^\dagger (s^{-1})	k_{-2}^\dagger ($\text{M}^{-1} \text{s}^{-1}$)	k_3^\dagger (s^{-1})
Native	$89 \pm 7^\ddagger/120^\S$	$0.93 \pm 0.05^\ddagger/1.0^\S$	$11 \pm 1^\ddagger$	1.3×10^8	1.8×10^6	1.7×10^7	2.0×10^8	1.2×10^6
V143I	$11 \pm 1^\ddagger/9.3 \pm 0.3^\S$	$1.0 \pm 0.2^\ddagger/0.7 \pm 0.1^\S$	$100 \pm 24^\ddagger$	—	—	—	—	—

[†] From Behravan *et al.* (1990). [‡] From Fierke *et al.* (1991). [§] From West *et al.* (2012).

the mouth of this pocket and forms van der Waals contacts with Leu198 and Trp209. W_{DW} occupies the pre-catalytic association site for substrate and is displaced by one of the O atoms of CO₂ during binding (Domsic *et al.*, 2008). The hydrophobic pocket residues are highly conserved and are known to be critical for CO₂ sequestration, although they do not directly interact with the CO₂ molecule.

Between the hydrophilic and hydrophobic sides of the active site, a cluster of ordered waters has recently been identified located near the active-site entrance, termed the entrance-conduit (EC) waters [Fig. 1(c)] (Kim *et al.*, 2018). This ordered water ensemble connects the active site to the external bulk solvent, creating a pathway where water, substrate and product can interchange and interact with bulk solvent. These EC waters are believed to be involved in water replenishment during catalysis, displacing the zinc-bound bicarbonate and restoring the proton-transfer water network.

In order to elucidate the catalytic details of the active site of CA II, several mutational studies have been performed. Most of these variants have been focused at the zinc ion-binding site (Alexander *et al.*, 1993; Kiefer *et al.*, 1993; Ippolito & Christianson, 1994; Lesburg & Christianson, 1995; Huang *et al.*, 1996; Lesburg *et al.*, 1997), the hydrophilic side (proton-transfer pathway; Behravan *et al.*, 1990; Krebs, Ippolito *et al.*, 1993; Xue *et al.*, 1993; Ippolito *et al.*, 1995; Huang *et al.*, 2002; Tu *et al.*, 2002; Fisher *et al.*, 2005; Zheng *et al.*, 2008; Turkoglu *et al.*, 2012; Mikulski *et al.*, 2013; Aggarwal *et al.*, 2014) and the hydrophobic pocket (CO₂-binding site; Alexander *et al.*, 1991; Fierke *et al.*, 1991; Nair *et al.*, 1991; Krebs, Rana *et al.*, 1993; West *et al.*, 2012; Nair & Christianson, 1993). In the hydrophobic pocket, a series of mutational studies have been performed targeting the Val121, Val143 and Leu198 residues. It was found that CA catalysis is severely compromised (an $\sim 10^4$ – 10^5 -fold decrease) when the deep water W_{DW} is displaced by replacement of the relevant amino acid by one with a larger side chain (for example, replacement of Val143 by Phe or Tyr), leading to a substantial blockage of CO₂ binding. On the other hand, some of the point mutations, such as Val121 to Ala, Val143 to Ile and Leu198 to Glu, do not directly displace W_{DW} and the CA catalysis is only moderately compromised (a fewfold to a 20-fold decrease). Understanding these moderate effects is most challenging as the overall structures and active sites show little deviation when compared with native CA II. It is expected that delicate perturbations are introduced at the level of intermediate structures during the moderately modified CA catalysis.

In this study, we investigate one of the most challenging cases and describe the subtle effects brought on by a Val143 to Ile (V143I) mutation. As shown in Table 1, the V143I variant

shows an approximately tenfold decrease in k_{cat}/K_m , while k_{cat} remains almost the same as that for native CA II. Structural analysis was performed by comparing the catalytic intermediate states of native and V143I CA II, which were obtained by cryocooling protein crystals under four different CO₂ pressures [ranging from 0 (no CO₂ pressurization) to 15 atm]. The intermediate states are henceforth referred to as native-0atm (PDB entry 6km3), native-7atm (PDB entry 6km4), native-13atm (PDB entry 6km5) and native-15atm (PDB entry 6km6) and as V143I-0atm (PDB entry 6klz), V143I-7atm (PDB entry 6km0), V143I-13atm (PDB entry 6km1) and V143I-15atm (PDB entry 6km2), respectively. Based upon the structural modifications, we successfully estimated the alterations in the reaction rate constants and the corresponding free-energy profiles in the CA II enzymatic mechanism. This study systematically reveals how a single point mutation influences an enzyme's catalytic pathway at the atomic level, leading to an estimation of the kinetics governing its individual mechanistic steps.

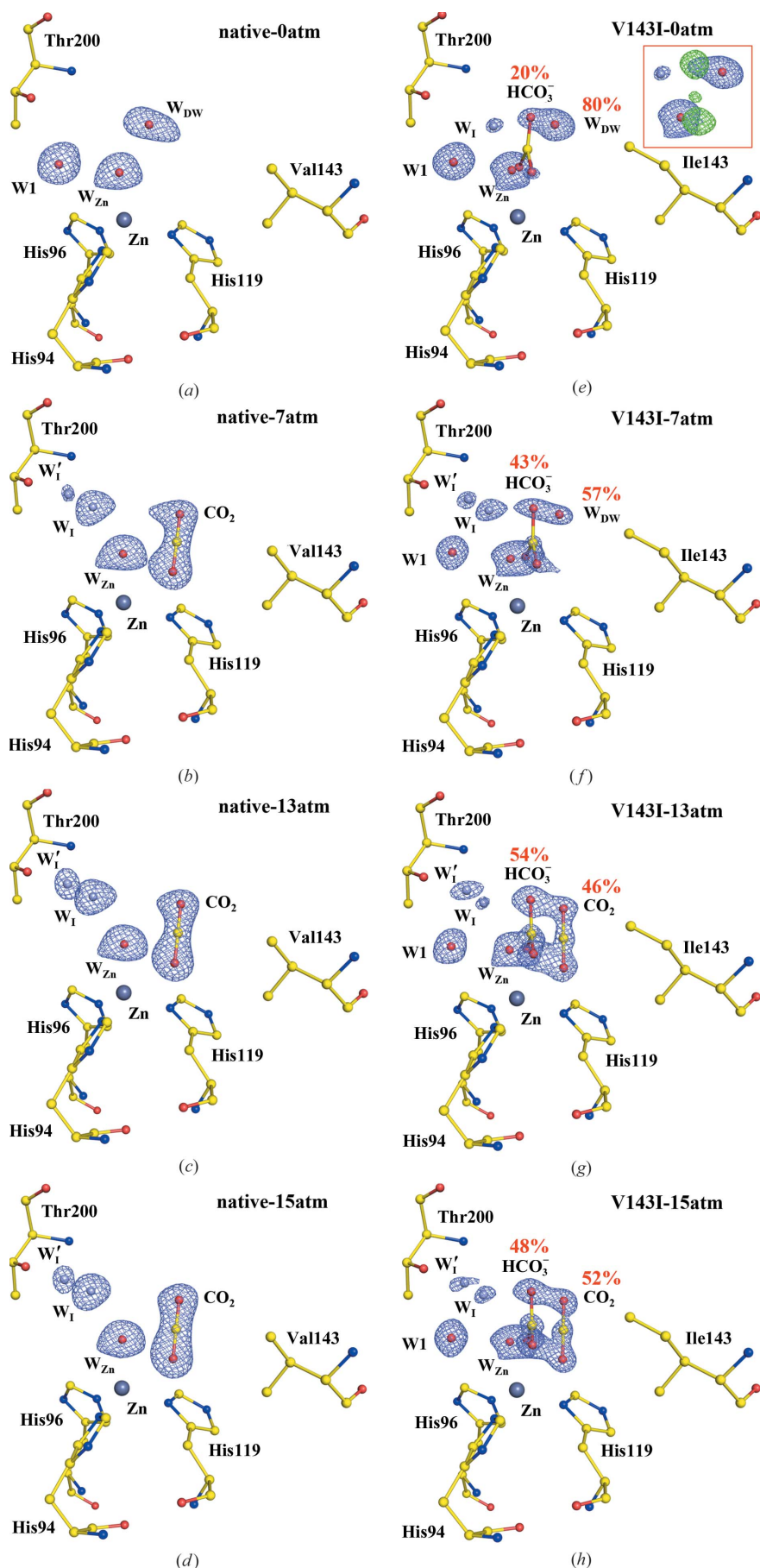
2. Results

Our X-ray studies (methods are reported in the supporting information) revealed that the overall protein backbones (tertiary structures) of the native and V143I CA II structures were very similar, with C^α–C^α r.m.s.d. values of less than 0.14 Å (Supplementary Tables S1 and S2). However, careful structural analysis successfully established subtle but clear changes in the active site (CO₂-binding site, proton-transfer pathway and water-replenishment pathway; EC waters). The key bound water molecules in native and V143I CA II are listed in Supplementary Tables S3 and S4.

2.1. CO₂-binding site around the zinc ion

Fig. 2 shows the CO₂-binding site and crucial water molecules (W_{Zn}/W_{DW}/W_I/W_I'/W₁) in the vicinity of the zinc ion. In native CA II [Figs. 2(a)–2(d)], the water molecules (W_{Zn}/W_{DW}/W₁) around the zinc ion are initially well ordered at 0 atm CO₂ pressure. At higher CO₂ pressures of 7–15 atm, electron density for the CO₂ molecule becomes apparent, displacing the deep water (W_{DW}). Concurrently, two intermediate waters W_I and W_I' emerge near Thr200, while W₁ disappears at higher CO₂ pressures. The distance between W_I and W₂ is ~ 4.7 Å, suggesting that the hydrogen-bonded water network that facilitates proton transfer is disrupted when the CO₂-binding site is fully occupied.

On the other hand, the active site of V143I CA II shows noteworthy modifications. The most striking difference is that HCO₃[−] is stabilized and is observable at 0 atm CO₂ pressure with an estimated occupancy of $\sim 20\%$ [Fig. 2(e)]. In the



absence of experimentally introduced CO_2 , it is likely that the captured HCO_3^- is converted from CO_2 absorbed into the crystal from ambient air. As the CO_2 pressure increases, the HCO_3^- occupancy increases to 54% at 13 atm and subsequently decreases slightly to 48% at 15 atm, with increased CO_2 occupancy [Figs. 2(f)–2(h)]. It is likely that the observed decrease in the HCO_3^- occupancy at 15 atm is owing to steric hindrance from the bound CO_2 molecule. When superimposed with the previously reported coordinates of HCO_3^- bound to native CA II (PDB entry 2vvb; Sjöblom *et al.*, 2009), the HCO_3^- position observed in V143I CA II shows noticeable deviations. The HCO_3^- molecule is tilted by 35° with respect to the plane containing W_{Zn} , CO_2 and HCO_3^- in native CA II (Supplementary Fig. S1). In addition, the central C atoms of the two superimposed HCO_3^- molecules in native and V143I CA II are separated by 0.5 Å.

Unlike the HCO_3^- molecule, the CO_2 molecule is less stable in V143I CA II. For example, CO_2 shows almost full occupancy at 7 atm in native CA II, while no CO_2 is visible at 7 atm in V143I CA II, which instead shows the appearance of W_{DW} [Figs. 2(b) and 2(f)]. The CO_2 molecule appears at higher pressures (13 and 15 atm) with a decreased occupancy of $\sim 50\%$ [Figs. 2(g) and 2(h)]. The bound CO_2 is tilted by $\sim 6^\circ$ and is situated closer to the zinc ion by 0.34 Å compared with that in native CA II (Supplementary Fig. S1). The distance between the end carbon ($\text{C}^{\delta 1}$) of Ile143 and the CO_2 molecule is only 3.0–3.2 Å, and this steric disruption seems to affect the critical interactions between the CO_2 molecule and the

Figure 2
 $\text{CO}_2/\text{HCO}_3^-$ -binding site of native and V143I CA II. The intermediate waters (W_1 and W_1') are coloured steel blue for clarity. The electron density ($2F_o - F_c$) is contoured at 1.5σ where not indicated otherwise. (a)–(d) Native CA II structures. (e)–(h) V143I CA II structures. W_1' at 7, 13 and 15 atm is contoured at 1.25σ and W_1 at 0 atm is contoured at 1.0σ . Partial occupancies of HCO_3^- and W_{DW} were determined in V143I-0atm and V143I-7atm, and partial occupancies of HCO_3^- and CO_2 were determined at the higher CO_2 pressures (see the supporting information). The inset (red box) in V143I-0atm shows the difference map ($F_o - F_c$ contoured at 3.0σ ; green) when the HCO_3^- molecule is not included in the structure refinement.

hydrophobic pocket, thereby destabilizing it in the active site. It is worth noting that in contrast to native CA II, the bound CO₂ molecule in V143I CA II is distorted from the plane defined by the bound HCO₃⁻ molecule, and this seems to be detrimental to the efficient conversion of CO₂ to HCO₃⁻.

Finally, the two intermediate waters W_I and W_I' show different behaviour in V143I CA II. The intermediate water W_I is visible even in 0 atm V143I CA II but is not present in 0 atm native CA II [Figs. 2(a) and 2(e)]. However, it is observed that the electron densities of the two intermediate

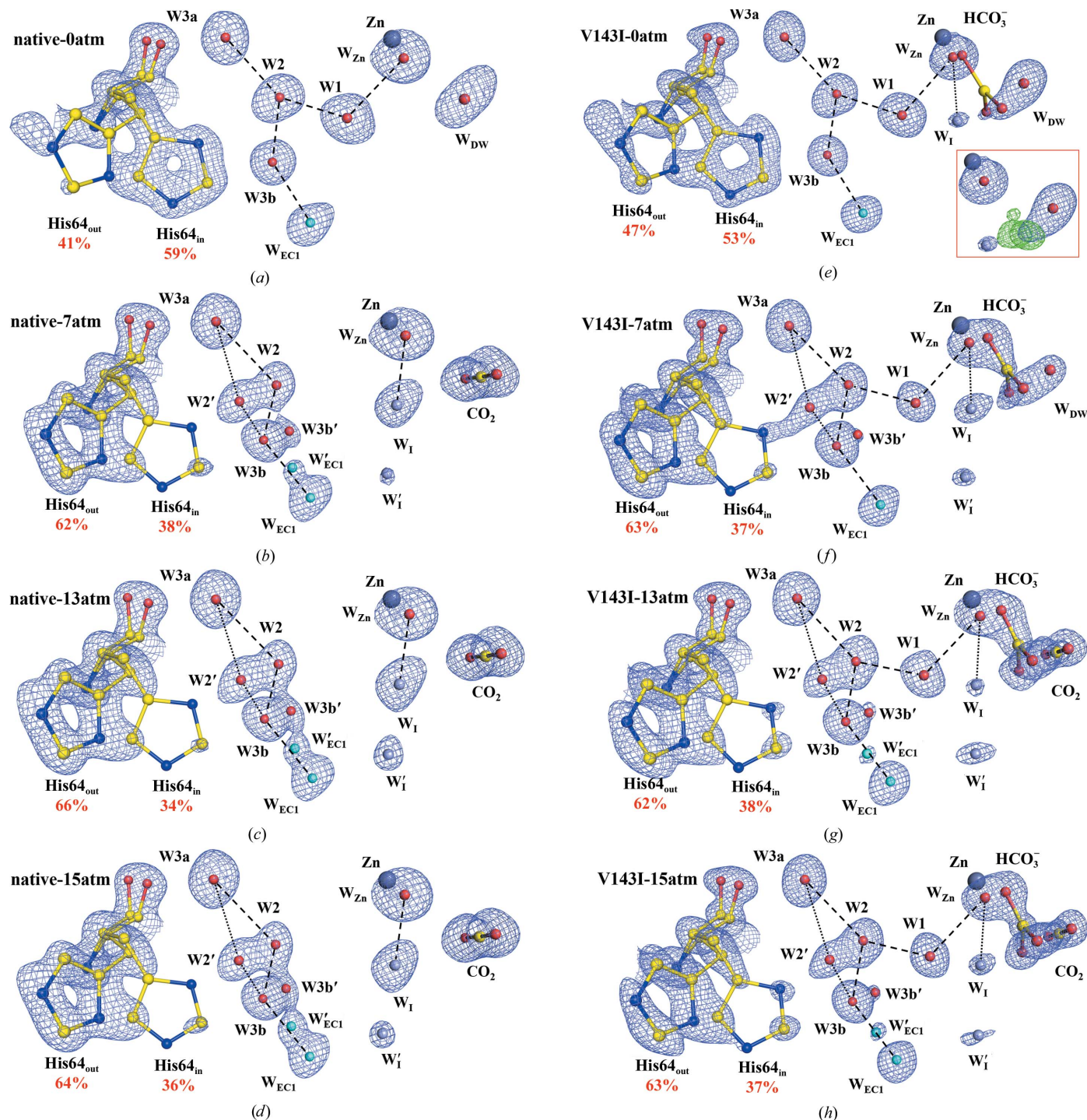


Figure 3 Proton-transfer pathway including the water network and His64. The entrance-conduit waters (W_{EC}) are coloured cyan and the intermediate waters (W_I and W_I') are coloured steel blue for clarity. The electron density ($2F_o - F_c$) is contoured at 1.5σ where not indicated otherwise. The major hydrogen bonds between water molecules are represented by dashed lines, while alternative hydrogen bonds that are mutually exclusive are represented by dotted lines. (a)–(d) Native CA II structures. (e)–(h) V143I CA II structures. W_I' at 7, 13 and 15 atm and W_{EC1}' at 15 and 13 atm are contoured at 1.25σ, and W_I at 0 atm is contoured at 1.0σ. The inset (red box) in V143I-0atm shows the difference map ($F_o - F_c$ contoured at 3.0σ; green) when the HCO₃⁻ molecule is not included in the structure refinement.

waters were less defined than in native CA II [Figs. 2(f)–2(h)]. These ‘weaker’ intermediate waters were accompanied by the presence of W1 at all pressures (0–15 atm). It is likely that these weak intermediate waters are related to the perturbed structures and dynamical motions of the EC waters, as explained later.

2.2. Proton-transfer pathway

Fig. 3 shows the proton-transfer pathway including the water network (W1/W2/W3a/W3b) and His64. In native CA II, the water network is initially well ordered at 0 atm CO₂ pressure [Fig. 3(a)]. As the CO₂ pressure increases, W1 disappears and intermediate waters (W_I and W_I') emerge instead [Figs. 3(b)–3(d)]. The W2 water, which transfers a proton from W1 to His64, shows an alternative position denoted W2'. Considering the steric hindrance between His64_{in} and W2', it seems that the presence of W2' pushes His64 towards the ‘out’ conformation (away from the water network). Indeed, His64 shows a net movement from the ‘in’ to the ‘out’ conformation as W2' becomes prominent at higher CO₂ pressures. W3a shows little change, but W3b shows an alternative water position, W3b', and is found to interact with one of the entrance waters W_{EC1} (and its alternative position W_{EC1}').

Similarly, in V143I CA II W2 shows the same alternative position W2', and His64 shows the same ‘in’ to ‘out’ flip, with similar occupancies as observed in native CA II with increasing CO₂ pressure [Figs. 3(e)–3(h)]. W3b and W_{EC1} also show the same alternative positions, although their electron densities are slightly weaker. As the distance between W2 and the N atom (N^{δ1}) of His64_{in} is relatively long (3.3 Å), efficient proton transfer seems to depend on the dynamical motions of W2/W2' and His64_{in}/His64_{out}. These motions are quite similar in native and V143I CA II and therefore proton transfer is not significantly impacted in the variant.

2.3. Water-replenishment pathway

Fig. 4 shows the water-replenishment pathway consisting of the ordered EC waters (W_{EC1}/W_{EC2}/W_{EC3}/W_{EC4}/W_{EC5}). In native CA II, the five W_{EC} waters are well ordered at 0 atm CO₂ pressure [Fig. 4(a)]. As the CO₂ pressure increases, W_{EC1} shows an alternative position W_{EC1}', and W_{EC2} shifts to an alternative position W_{EC2}' [Figs. 4(b)–4(d)]. These dynamical motions of W_{EC1} and W_{EC2} are accompanied by the emergence of the intermediate waters W_I and W_I'. The two intermediate waters are located deep within the entrance conduit near the active site and are transiently stabilized via hydrogen bonding to several W_{EC} waters (W_{EC2}, W_{EC3} and W_{EC5} and their alternative positions). The short distance (2.2 Å) between W_I and W_I' suggests that W_I' can rapidly shift to the W_I position as W_I refills the vacant water positions (W1/W_{Zn}/W_{DW}) during catalysis. Previous studies suggest that the intermediate waters (W_I and W_I') play a critical role in the rapid replenishment of the active-site water network during catalysis and therefore could influence the overall catalytic rate (Kim *et al.*, 2018).

Among the five W_{EC} waters in V143I CA II, W_{EC2} is located close to the mutated residue Ile143. Indeed, the W_{EC1} to W_{EC4} waters show similar structures and dynamical motions as in native CA II, but W_{EC2} shows a significantly distinct behaviour. Initially, at 0 atm CO₂ pressure, the W_{EC2} water shows multiple alternative positions (W_{EC2}'', W_{EC2}'''' and W_{EC2}'''') [Fig. 4(e)]. As the CO₂ pressure increases, these alternative positions disappear and both the W_{EC2} and W_{EC2}' waters are observed instead [Figs. 4(f)–4(h)]. Compared with native CA II, W_{EC2}'', W_{EC2}'''' and W_{EC2}''''' are new alternative positions that are observed only at 0 atm CO₂ pressure in V143I CA II. Along with the perturbed dynamical motions of the W_{EC2} water, much weakened electron densities of the intermediate waters W_I and W_I' are observed. It should be noted that among the five EC waters, W_{EC2} is unique in that it interacts with all three of the key waters, W1, W_I and W_I'. Therefore, the fact that the structures and dynamical motions of the W_{EC2} waters are significantly perturbed in V143I CA II is likely to account for the stabilization of W1 but the destabilization of the two intermediate waters.

Another interesting aspect of W_{EC2} is that its alternative position W_{EC2}''''' is situated close to the bound HCO₃⁻. The distances between W_{EC2}''''' and the closest O atom and the C atom of HCO₃⁻ are 1.4 and 2.5 Å, respectively (Supplementary Table S5). Since W_{EC2}''''' is too close to the bound HCO₃⁻, W_{EC2}''''' and HCO₃⁻ cannot coexist in tandem. Indeed, W_{EC2}''''' is only visible in V143I CA II at 0 atm, when the HCO₃⁻ occupancy is low, and disappears as the HCO₃⁻ occupancy increases at higher CO₂ pressures [Figs. 4(e)–4(h)]. It seems that the relationship between W_{EC2}''''' and HCO₃⁻ is analogous to the relationship between W_{DW} and CO₂. In native CA II, the hydrophobic cavity produces an electrostatic environment in which the deep water (W_{DW}) can be locally stabilized around the zinc ion and then replaced with one of the O atoms of CO₂ upon CO₂ binding. In V143I CA II, the altered hydrophobic cavity owing to the V143I mutation produces a slightly different electrostatic environment in which an additional water position (W_{EC2}'''') can be locally stabilized around the zinc ion and subsequently replaced with one of the O atoms in HCO₃⁻ during CA II catalysis. The release of the W_{EC2}''''' molecule upon HCO₃⁻ binding seems to reduce the entropic cost of the process, analogous to the release of W_{DW} upon CO₂ binding in native CA II. Thus, it is likely that the altered multiple conformations of W_{EC2} allow HCO₃⁻ to bind more easily and firmly in a tilted configuration at the active site.

3. Discussion

In this study, we have successfully identified the ‘fine’ structural changes in the CA II intermediates induced by a single-residue mutation at the active site. The V143I mutation in CA II produces steric hindrance and induces subtle changes in the electrostatic environment of the active site. The resulting effects on the CA II intermediates can be summarized as follows: (i) the dynamical motions and the allowed configurations of CO₂ are slightly restricted and the binding affinity of HCO₃⁻ is increased with a distorted configuration and (ii)

the EC water network in the water-replenishment pathway is restructured, while (iii) the proton-transfer dynamics are

mostly unaffected. These detailed structural insights can now be used to assess the modifications in the reaction rate

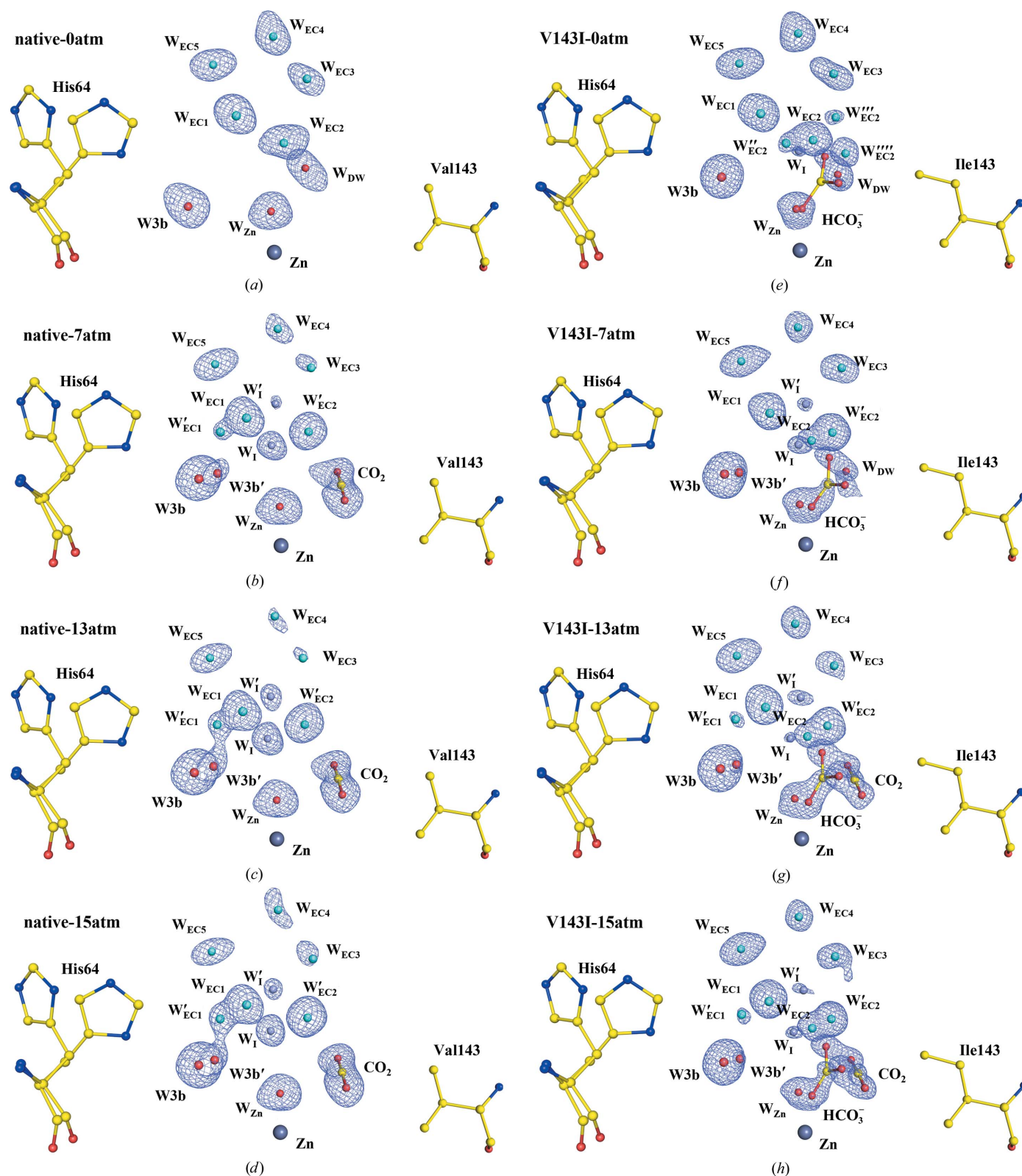


Figure 4
 The water-replenishment pathway including entrance-conduit waters (cyan) and intermediate waters (steel blue). The electron density ($2F_o - F_c$) is contoured at 1.5σ where not indicated otherwise. (a)–(d) Native CA II structures. W_{EC3} at 7 and 13 atm and W_{EC4} at 15 atm are contoured at 1.25σ , and W_{EC3} at 15 atm is contoured at 1.0σ . (e)–(h) V143I CA II structures. W'_I at 7, 13 and 15 atm and W''_{EC1} at 15 and 13 atm are contoured at 1.25σ and W_I at 0 atm is contoured at 1.0σ . Compared with native CA II, V143I CA II shows significantly perturbed positions for W_{EC2} .

constants (k_1 , k_{-1} , k_2 and k_3) and the corresponding free-energy profiles during the CO₂-hydration reaction of CA II.

Firstly, the V143I mutation restricts the configurational freedom of the CO₂ molecule within the hydrophobic pocket of CA II. Previous mutational studies on hydrophobic pocket residues (Val121 and Val143) suggest that the hydrophobic pocket of native CA II is involved in ‘ushering’ the CO₂ molecule to the zinc hydroxide in the active site, but does not directly interact with the CO₂ molecule to hold it in a specific orientation. Therefore, it is most likely that the CO₂ molecule in aqueous solution is guided to the hydrophobic pocket of CA II but retains some degrees of freedom with regard to the acceptable configurations (positions and orientations) around the zinc hydroxide that eventually facilitate its rapid conversion into HCO₃⁻. In the V143I variant, although the hydrophobicity of the active-site pocket is increased, the added methyl group appears to sterically restrict the number of favourable configurations and the dynamical motions accessible to the CO₂ molecule within the cavity. This estimation is supported by the crystallographic observation that the CO₂ molecule is distorted towards the zinc ion, tilted by ~6° and is destabilized with lower occupancies in the V143I variant. Consequently, interconversion from CO₂ to HCO₃⁻ becomes less efficient, leading to a reduced k_1 ($k_1^{V143I} < k_1^{\text{native}}$). The lower k_1 value also implies an enhanced activation-energy barrier for the step [Arrhenius relationship: $k_1(T) = A \exp(-E_1/RT)$, where A is a pre-exponential constant, R is the molar gas constant, T is the absolute temperature and E_1 is the activation energy] (Fig. 5).

Secondly, the V143I mutation induces a slightly different electrostatic environment in the hydrophobic cavity, thereby altering the location and dynamics of the W_{EC2} water. It seems that one of these altered W_{EC2} waters (W_{EC2}^{''''}) increases the binding affinity of the HCO₃⁻ molecule in the active site. This stronger binding of HCO₃⁻ suggests that the free energy of the

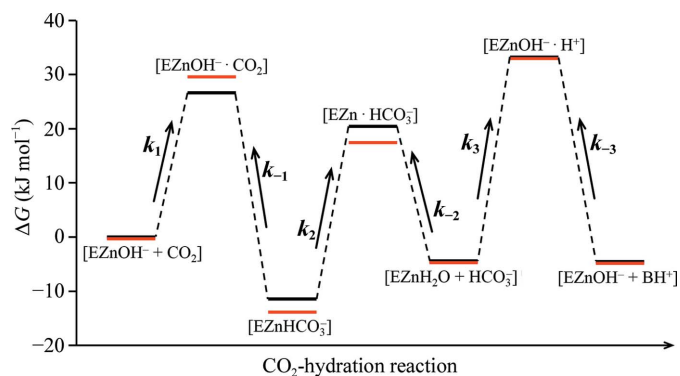


Figure 5

Estimated free-energy profiles for the CO₂-hydration reaction catalyzed by CA II. The energy states of native CA II (black) are from a previous study (Behravan *et al.*, 1990). The energy states of V143I CA II (red) are qualitatively estimated with respect to the native form by considering the structural information and the variations in the reaction rate constants. Note that the energy level of [EZnH₂O + HCO₃⁻] in the V143I variant is assumed to be the same as that in native CA II. The depicted energy gaps are not to scale.

enzyme–product (EZnHCO₃⁻) complex is lowered in the V143I variant (Fig. 5). In conjunction with the larger activation energy for the k_1 reaction, it can be deduced that the activation energy for the reverse reaction k_{-1} is increased even further, leading to a reduced k_{-1} value ($k_{-1}^{V143I} < k_{-1}^{\text{native}}$). On the other hand, the alterations of the W_{EC2} water in the V143I variant make the intermediate waters (W_I and W_I[']) slightly less stable, therefore possibly slowing down the replenishment of the active-site water network and HCO₃⁻ dissociation. This results in a reduced k_2 value ($k_2^{V143I} < k_2^{\text{native}}$).

Thirdly, the V143I mutation seems to have little effect on the kinetics of the proton-transfer reaction. It is observed that W_I is more stabilized in the V143I variant intermediates. It should be noted that the intermolecular proton transfer can occur via the fully established water network W_{Zn} → W_I → W₂ → His64. This implies that if a mutation induces the destabilization of W_I, proton transfer could be significantly perturbed. However, stabilization of W_I as in the V143I variant does not necessarily suggest a faster proton-transfer process. Rather, it is the dynamical motions of W₂ and His64 that have a more critical influence on the proton-transfer rate. Our results suggest that both W₂ and His64 show very similar dynamical motions. Taken together, it seems that the overall proton-transfer rate k_3 is not significantly altered in the V143I mutant ($k_3^{V143I} \simeq k_3^{\text{native}}$).

The interplay between the modified reaction rate constants, as discussed above, now allows us to determine the effect of the V143I mutation on the measured kinetic parameters (k_{cat} and k_{cat}/K_m ; Nair *et al.*, 1991; Krebs, Ippolito *et al.*, 1993). The steady-state kinetic parameters for the CO₂-hydration reaction are listed in Table 1. The k_{cat} value shows little change, but the second-order rate constant k_{cat}/K_m shows an approximately tenfold decrease in the V143I variant. The parameter k_{cat} contains rate constants from the initial enzyme–substrate complex through the remaining steps, including proton transfer. Therefore, for the proposed mechanistic scheme (equations 1 and 2), k_{cat} can effectively be represented as $k_{\text{cat}} = k_2 k_3 / (k_2 + k_3)$. On the other hand, the ratio k_{cat}/K_m contains rate constants for the initial association of the substrate CO₂ through the dissociation of the product HCO₃⁻. Hence, k_{cat}/K_m only contains rate constants from equation 1 (and not equation 2) and is represented as $k_{\text{cat}}/K_m = k_1 k_2 / (k_{-1} + k_2)$.

It is known that in native CA II the HCO₃⁻-dissociation process (k_2) is much faster than the reverse interconversion from HCO₃⁻ to CO₂ (k_{-1}) and the proton-transfer rate (k_3), *i.e.* $k_2^{\text{native}} \gg k_{-1}^{\text{native}}$, $k_2^{\text{native}} \gg k_3^{\text{native}}$, with $k_2^{\text{native}} \simeq 10k_{-1}^{\text{native}}$, $k_2^{\text{native}} \simeq 15k_3^{\text{native}}$ and $k_{-1}^{\text{native}} \simeq 1.5k_3^{\text{native}}$ (Table 1). Combining this information with the insights gleaned from our study ($k_1^{V143I} < k_1^{\text{native}}$, $k_{-1}^{V143I} < k_{-1}^{\text{native}}$, $k_2^{V143I} < k_2^{\text{native}}$ and $k_3^{V143I} \simeq k_3^{\text{native}}$), we can estimate the effect of the V143I point mutation on the observed kinetic parameter k_{cat} in the following way. In the native state $[k_{\text{cat}}]^{\text{native}} = k_2^{\text{native}} k_3^{\text{native}} / (k_2^{\text{native}} + k_3^{\text{native}}) \simeq k_3^{\text{native}}$ (using $k_2^{\text{native}} \gg k_3^{\text{native}}$), indicating that the turnover rate in the native is almost the same as the proton-transfer rate and that the proton-transfer process is the rate-limiting step. In the V143I variant $[k_{\text{cat}}]^{V143I} = k_2^{V143I} k_3^{V143I} / (k_2^{V143I} + k_3^{V143I}) \simeq k_3^{V143I} [k_2^{V143I} / (k_2^{V143I} + k_3^{V143I})]$ (using $k_3^{V143I} \simeq k_3^{\text{native}}$), and the

experimental measurement (Table 1) suggests that $[k_{\text{cat}}]^{V143I} \simeq [k_{\text{cat}}]^{\text{native}} \simeq k_3^{\text{native}}$, implying that $[k_2^{V143I}/(k_2^{V143I} + k_3^{V143I})] \simeq 1$, or $k_2^{V143I} \gg k_3^{V143I}$. This result indicates that HCO_3^- dissociation (k_2) remains faster than proton transfer (k_3) in the V143I variant and that the proton-transfer process is still the rate-limiting step in the V143I variant. The negligible reduction in k_2^{V143I} suggests that its activation energy is not significantly increased (Fig. 5).

The second-order rate constant k_{cat}/K_m shows the following relationship in the native state: $[k_{\text{cat}}/K_m]^{\text{native}} = k_1^{\text{native}}k_2^{\text{native}}/(k_{-1}^{\text{native}} + k_2^{\text{native}}) \simeq k_1^{\text{native}}$ (using $k_2^{\text{native}} \gg k_{-1}^{\text{native}}$). This indicates that $[k_{\text{cat}}/K_m]^{\text{native}}$ mostly reflects the CO_2 -binding step and its interconversion to HCO_3^- . On the other hand, in the V143I variant both the dissociation of HCO_3^- (k_2) and the reverse interconversion (k_{-1}) from HCO_3^- to CO_2 are retarded ($k_2^{V143I} < k_2^{\text{native}}$ and $k_{-1}^{V143I} < k_{-1}^{\text{native}}$), leaving the relation $k_2^{V143I} \gg k_{-1}^{V143I}$ unresolved. However, the relation $k_2^{V143I} \gg k_3^{V143I} \simeq k_3^{\text{native}}$ obtained from the k_{cat} analysis above suggests that k_2^{V143I} is still an order of magnitude larger than k_3^{native} , while $k_{-1}^{V143I} < k_{-1}^{\text{native}} \simeq 1.5k_3^{\text{native}}$ suggests that k_{-1}^{V143I} is comparable to or less than k_3^{native} , thereby ensuring that the relation $k_2^{V143I} \gg k_{-1}^{V143I}$ remains valid. Thus, we can estimate the k_{cat}/K_m in the V143I variant in the following manner: $[k_{\text{cat}}/K_m]^{V143I} = k_1^{V143I}k_2^{V143I}/(k_{-1}^{V143I} + k_2^{V143I}) \simeq k_1^{V143I}$ (using $k_2^{V143I} \gg k_{-1}^{V143I}$). This estimation indicates that the reduced $[k_{\text{cat}}/K_m]^{V143I}$ is mostly owing to the decrease in k_1 , reflecting the slower CO_2 binding and interconversion to HCO_3^- in the V143I variant. It should be noted that the reduction in the k_{-1} value has little effect on $[k_{\text{cat}}/K_m]^{V143I}$ in the direction of CO_2 hydration, as long as the reduction in k_2 is small enough to keep the relation $k_2^{V143I} \gg k_{-1}^{V143I}$ valid. However, it is expected that the reduction in the k_{-1} value would have significant consequences for the HCO_3^- -dehydration direction.

Finally, considering that $k_{\text{cat}} \simeq k_3$ and $[k_{\text{cat}}/K_m] \simeq k_1$ in both native and V143I CA II, the Michaelis constant K_m is expressed in the following way: $K_m^{\text{native}} = k_3^{\text{native}}/k_1^{\text{native}}$ and $K_m^{V143I} = k_3^{V143I}/k_1^{V143I}$. Consequently, $K_m^{V143I} > K_m^{\text{native}}$ can be obtained using the estimated relationships $k_1^{V143I} < k_1^{\text{native}}$ and $k_3^{V143I} \simeq k_3^{\text{native}}$. The relationship shows that the substrate concentration needed to reach half of the maximum reaction velocity is larger in V143I CA II mainly owing to the slower CO_2 binding and interconversion to HCO_3^- .

Although our study was performed for a single point mutation within the hydrophobic pocket (V143I), our approach and interpretations can be extended to arbitrary mutations in CA II. Considering the forward CO_2 -hydration direction, the mutation can first perturb substrate funnelling into the hydrophobic pocket via steric hindrance, thereby limiting the configurations that allow its efficient conversion into product. This influence is directly reflected in k_{cat}/K_m , but not in k_{cat} . Secondly, the mutation can structurally distort the proton-transfer pathway by perturbing the water network or its associated stabilizing residues, and this effect is directly reflected in k_{cat} but not in k_{cat}/K_m . Thirdly, the mutation can alter the product-dissociation process via direct steric hindrance or perturbations in the water-replenishment pathway. This influence can be intricate and is reflected both in

k_{cat} and k_{cat}/K_m . On the other hand, the mutation can affect the reverse reaction, the interconversion from product to substrate and substrate dissociation, but this has little influence on either k_{cat} or k_{cat}/K_m in the hydration direction, as long as the reverse interconversion process is much slower than the product-dissociation process.

4. Conclusion

We systematically studied the effect of a single-residue mutation on the CA II catalytic pathway at atomic resolution. We have successfully captured the high-resolution intermediate states of the V143I variant and shown clearly that the single point mutation induces noticeable changes in substrate and product binding at the active site and in the water-replenishment pathway, but has little effect on the proton-transfer pathway. The structural information was then utilized to estimate the reaction rate constants and the free-energy profiles during the catalytic cycle, unravelling the effect of the point mutation on the altered kinetic parameters. We believe that the detailed and systematic approach in our CA II study can be extended to identify the specific roles of target amino-acid residues in many other biologically important enzymes. We also anticipate that our detailed descriptions could serve as a reference point for future theoretical and computational studies that may lead to an advanced understanding of enzyme mechanisms at the quantum-chemistry level.

5. Related literature

The following references are cited in the supporting information for this article: Emsley *et al.* (2010), Forsman *et al.* (1988), Henderson (1990), Khalifah *et al.* (1977), Kim *et al.* (2005, 2006, 2013, 2016), McPherson (1982), Murshudov *et al.* (2011), Otwinowski & Minor (1997) and Winn *et al.* (2011).

Acknowledgements

The authors would like to thank the staff at Pohang Light Source II and Cornell High Energy Synchrotron Source for their support during data collection. CHESS is supported by the NSF and NIH/NIGMS via NSF award DMR-1829070 and the MacCHESS resource is supported by NIH/NIGMS award GM-124166. Authors contributions were as follows. CUK conceived the research. JKK, CL, SWL, JTA and AA ran the experiments. JKK and CUK analyzed the data. JKK, JTA, RM and CUK wrote the manuscript. All authors contributed to the overall scientific interpretation and edited the manuscript.

Funding information

This work was supported by the Basic Science Research Program through the National Research Foundation of Korea (2019R1A2C1004274).

References

- Aggarwal, M., Kondeti, B., Tu, C., Maupin, C. M., Silverman, D. N. & McKenna, R. (2014). *IUCrJ*, **1**, 129–135.
- Alexander, R. S., Kiefer, L. L., Fierke, C. A. & Christianson, D. W. (1993). *Biochemistry*, **32**, 1510–1518.
- Alexander, R. S., Nair, S. K. & Christianson, D. W. (1991). *Biochemistry*, **30**, 11064–11072.
- Behravan, G., Jonsson, B.-H. & Lindskog, S. (1990). *Eur. J. Biochem.* **190**, 351–357.
- Chegwidden, W. R., Carter, N. D. & Edwards, Y. H. (2013). *The Carbonic Anhydrases: New Horizons*. Basel: Birkhäuser.
- Christianson, D. W. & Fierke, C. A. (1996). *Acc. Chem. Res.* **29**, 331–339.
- Davenport, H. W. (1984). *Ann. NY Acad. Sci.* **429**, 4–9.
- Domsic, J. F., Avvaru, B. S., Kim, C. U., Gruner, S. M., Agbandje-McKenna, M., Silverman, D. N. & McKenna, R. (2008). *J. Biol. Chem.* **283**, 30766–30771.
- Domsic, J. F. & McKenna, R. (2010). *Biochim. Biophys. Acta*, **1804**, 326–331.
- Emsley, P., Lohkamp, B., Scott, W. G. & Cowtan, K. (2010). *Acta Cryst. D* **66**, 486–501.
- Fersht, A. (1999). *Structure and Mechanism in Protein Science: A Guide to Enzyme Catalysis and Protein Folding*. New York: Freeman.
- Fierke, C. A., Calderone, T. L. & Krebs, J. F. (1991). *Biochemistry*, **30**, 11054–11063.
- Fisher, S. Z., Kovalevsky, A. Y., Domsic, J. F., Mustyakimov, M., McKenna, R., Silverman, D. N. & Langan, P. A. (2010). *Biochemistry*, **49**, 415–421.
- Fisher, S. Z., Maupin, C. M., Budayova-Spano, M., Govindasamy, L., Tu, C., Agbandje-McKenna, M., Silverman, D. N., Voth, G. A. & McKenna, R. (2007). *Biochemistry*, **46**, 2930–2937.
- Fisher, S. Z., Tu, C., Bhatt, D., Govindasamy, L., Agbandje-McKenna, M., McKenna, R. & Silverman, D. N. (2007). *Biochemistry*, **46**, 3803–3813.
- Fisher, Z., Hernandez Prada, J. A., Tu, C., Duda, D., Yoshioka, C., An, H., Govindasamy, L., Silverman, D. N. & McKenna, R. (2005). *Biochemistry*, **44**, 1097–1105.
- Forsman, C., Behravan, G., Osterman, A. & Jonsson, B.-H. (1988). *Acta Chem. Scand. B*, **42**, 314–318.
- Frey, P. A. & Hegeman, A. D. (2007). *Enzymatic Reaction Mechanisms*. Oxford University Press.
- Frost, S. C. & McKenna, R. (2013). *Carbonic Anhydrase: Mechanism, Regulation, Links to Disease, and Industrial Applications*. Dordrecht: Springer Science+Business Media.
- Henderson, R. (1990). *Proc. R. Soc. Lond. B*, **241**, 6–8.
- Huang, C.-C., Lesburg, C. A., Kiefer, L. L., Fierke, C. A. & Christianson, D. W. (1996). *Biochemistry*, **35**, 3439–3446.
- Huang, S., Sjöblom, B., Sauer-Eriksson, A. E. & Jonsson, B.-H. (2002). *Biochemistry*, **41**, 7628–7635.
- Ippolito, J. A., Baird, T. T. Jr, McGee, S. A., Christianson, D. W. & Fierke, C. A. (1995). *Proc. Natl Acad. Sci. USA*, **92**, 5017–5021.
- Ippolito, J. A. & Christianson, D. W. (1994). *Biochemistry*, **33**, 15241–15249.
- Ishida, T. (2010). *J. Am. Chem. Soc.* **132**, 7104–7118.
- Jencks, W. P. (1987). *Catalysis in Chemistry and Enzymology*. Mineola: Dover.
- Khalifah, R. G., Strader, D. J., Bryant, S. H. & Gibson, S. M. (1977). *Biochemistry*, **16**, 2241–2247.
- Kiefer, L. L., Ippolito, J. A., Fierke, C. A. & Christianson, D. W. (1993). *J. Am. Chem. Soc.* **115**, 12581–12582.
- Kim, C. U., Hao, Q. & Gruner, S. M. (2006). *Acta Cryst. D* **62**, 687–694.
- Kim, C. U., Kapfer, R. & Gruner, S. M. (2005). *Acta Cryst. D* **61**, 881–890.
- Kim, C. U., Song, H., Avvaru, B. S., Gruner, S. M., Park, S. & McKenna, R. (2016). *Proc. Natl Acad. Sci. USA*, **113**, 5257–5262.
- Kim, C. U., Wierman, J. L., Gillilan, R., Lima, E. & Gruner, S. M. (2013). *J. Appl. Cryst.* **46**, 234–241.
- Kim, J. K., Lomelino, C. L., Avvaru, B. S., Mahon, B. P., McKenna, R., Park, S. & Kim, C. U. (2018). *IUCrJ*, **5**, 93–102.
- Krebs, J. F., Ippolito, J. A., Christianson, D. W. & Fierke, C. A. (1993). *J. Biol. Chem.* **268**, 27458–27466.
- Krebs, J. F., Rana, F., Dluhy, R. A. & Fierke, C. A. (1993). *Biochemistry*, **32**, 4496–4505.
- Krishnamurthy, V. M., Kaufman, G. K., Urbach, A. R., Gitlin, I., Gudiksen, K. L., Weibel, D. B. & Whitesides, G. M. (2008). *Chem. Rev.* **108**, 946–1051.
- Lesburg, C. A. & Christianson, D. W. (1995). *J. Am. Chem. Soc.* **117**, 6838–6844.
- Lesburg, C. A., Huang, C.-C., Christianson, D. W. & Fierke, C. A. (1997). *Biochemistry*, **36**, 15780–15791.
- Liang, J. Y. & Lipscomb, W. N. (1990). *Proc. Natl Acad. Sci. USA*, **87**, 3675–3679.
- Maupin, C. M. & Voth, G. A. (2007). *Biochemistry*, **46**, 2938–2947.
- McPherson, A. (1982). *Preparation and Analysis of Protein Crystals*. Chichester: John Wiley & Sons.
- Mikulski, R., West, D., Sippel, K. H., Avvaru, B. S., Aggarwal, M., Tu, C., McKenna, R. & Silverman, D. N. (2013). *Biochemistry*, **52**, 125–131.
- Murshudov, G. N., Skubák, P., Lebedev, A. A., Pannu, N. S., Steiner, R. A., Nicholls, R. A., Winn, M. D., Long, F. & Vagin, A. A. (2011). *Acta Cryst. D* **67**, 355–367.
- Nair, S. K., Calderone, T. L., Christianson, D. W. & Fierke, C. A. (1991). *J. Biol. Chem.* **266**, 17320–17325.
- Nair, S. K. & Christianson, D. W. (1991). *J. Am. Chem. Soc.* **113**, 9455–9458.
- Nair, S. K. & Christianson, D. W. (1993). *Biochemistry*, **32**, 4506–4514.
- Otwinowski, Z. & Minor, W. (1997). *Methods Enzymol.* **276**, 307–326.
- Silverman, D. N. & Lindskog, S. (1988). *Acc. Chem. Res.* **21**, 30–36.
- Silverman, D. N. & McKenna, R. (2007). *Acc. Chem. Res.* **40**, 669–675.
- Sjöblom, B., Polentarutti, M. & Djinovic-Carugo, K. (2009). *Proc. Natl Acad. Sci. USA*, **106**, 10609–10613.
- Steiner, H., Jonsson, B.-H. & Lindskog, S. (1975). *Eur. J. Biochem.* **59**, 253–259.
- Supuran, C. T. & De Simone, G. (2015). *Carbonic Anhydrases as Biocatalysts: From Theory to Medical and Industrial Applications*. Amsterdam: Elsevier.
- Tu, C., Qian, M., An, H., Wadhwa, N. R., Duda, D., Yoshioka, C., Pathak, Y., McKenna, R., Laipis, P. J. & Silverman, D. N. (2002). *J. Biol. Chem.* **277**, 38870–38876.
- Tu, C. K., Silverman, D. N., Forsman, C., Jonsson, B.-H. & Lindskog, S. (1989). *Biochemistry*, **28**, 7913–7918.
- Turkoglu, S., Maresca, A., Alper, M., Kockar, F., Işık, S., Sinan, S., Ozensoy, O., Arslan, O. & Supuran, C. T. (2012). *Bioorg. Med. Chem.* **20**, 2208–2213.
- West, D., Kim, C. U., Tu, C., Robbins, A. H., Gruner, S. M., Silverman, D. N. & McKenna, R. (2012). *Biochemistry*, **51**, 9156–9163.
- Winn, M. D., Ballard, C. C., Cowtan, K. D., Dodson, E. J., Emsley, P., Evans, P. R., Keegan, R. M., Krissinel, E. B., Leslie, A. G. W., McCoy, A., McNicholas, S. J., Murshudov, G. N., Pannu, N. S., Potterton, E. A., Powell, H. R., Read, R. J., Vagin, A. & Wilson, K. S. (2011). *Acta Cryst. D* **67**, 235–242.
- Xue, Y., Vidgren, J., Svensson, L. A., Liljas, A., Jonsson, B.-H. & Lindskog, S. (1993). *Proteins*, **15**, 80–87.
- Zheng, J., Avvaru, B. S., Tu, C., McKenna, R. & Silverman, D. N. (2008). *Biochemistry*, **47**, 12028–12036.